

tmp title: MUSC source

Damien Pageot^{*†}, Donatienne Leparoux^{*}, Mathieu Le Feuvre^{*}, Olivier

Durand^{*} and Yann Capdeville[†]

^{*}*LUNAM-IFSTTAR*,

[†]*OSUNA*

^{*}*LPGN*,

(September 18, 2015)

GEO-Example

Running head: *Geophysics example*

ABSTRACT

INTRODUCTION

Since the early developments of seismic imaging methods in the middle of 20th century, approaches and algorithms innovations are still proposed in current research projects. The improvements deal with both the qualitative imaging techniques like migration (e.g. Berkhout et al. (2012); Guofeng et al. (2013)), novel applications of quantitative imaging methods such as the first arrival tomography (e.g. Bohm et al. (2015)), or even more recent approaches like the Full Waveform Inversion (e.g. Perez Solano et al. (2014), see Virieux and Operto (2009) for a revue of this last decade). The refinements are proposed for different scales like near surface applications for civil engineering topics or more deeper investigation for example for oil prospection or crustal imaging at regional or global scales They are mostly validate by using synthetic data, for examples with well known shared benchmark (like the Marmousi case). However, the synthetic data are generally computed using the same wave propagation modeling engine used in the inverse problem process. In other terms, the synthetic data are computed with some assumptions which are the same in the inverse problem, for example the approximation of acoustic propagation, a 2D space medium, or a 2D cylindric source.

The best way to satisfy this need is to use Physical Small Scale Modeling Methods (noted *PSM* subsequently). *PSM* were used since several years to study the propagation of waves in various media with several stage of complexity, from acoustic wave propagation in homogeneous media to elastic wave propagation in three-dimensional heterogeneous anisotropic media (Rieber, 1936; Howes et al., 1953; Hilterman, 1970; French, 1974; Bishop et al., 1985; Pratt, 1999; Favretto-Cristini et al., 2013; Sarkar et al., 2003; Isaac and Lawton, 1999), and allow to generate experimental seismic data under well-controlled conditions. Some

methods exist to produce this kind of data for different purpose (Wong et al., 2009) and the MUSC system (Bretaudeau et al., 2008, 2011, 2013), *Mesure Ultrasonore Sans Contact* in French, in one of them. MUSC system is designed to allow (1) wide-angle on-shore acquisitions modeling both body waves and surface waves, (2) automatic multisource-multireceiver measurements with a high-productivity, (3) high-precision source-receiver positioning and (4) high-precision recording of absolute surface displacement without coupling effects.

Our objective here is to increase the potential of the MUSC system as a reliable tool for generating experimental data which will be distributed in the scientific community. Thus, we present two studies of experimental data in order to : 1) refine the comparison between numerical and experimental data by taking into account the 3D/2D geometrical spreading effects through an alternative way and 2) identify the reproducibility of the source impact and, consequently, data repeatability. These approaches will complete the knowledge of the system and facilitate the achievement of massive multi-source and multi-receiver data simulating subsurface seismic experimental campaigns.

To achieve some of these objectives, we used a seismic wave modeling code based on the Spectral Element Method (Komatitsch et al., 1998; Komatitsch and Tromp, 1999; Komatitsch et al., 2005; Festa and Vilotte, 2005). This method has several advantages compared to finite differences and finite elements, such as: (1) a weak formulation which can naturally take into account the free surface, (2) an explicit scheme in time facilitating parallelization and reducing the computational cost, (3) a spatial discretization (mesh) convenient for the representation of complex environments and (4) high precision results and low numerical dispersion.

Thus, this article is organized as follow. In a first part, we present the MUSC system and

the SEM code used for these studies. In a second part, we present two coupled studies of experimental data in order to: (1) refine the comparison between numerical and experimental data by taking into account the geometrical spreading effects between two-dimensional and three-dimensional data through an alternative way, and (2) identify the reproducibility of the source impact to validate the data reproducibility.

METHODS

Physical modeling: MUSC system

The MUSC system (Bretaudeau et al., 2008, 2011, 2013) is built to experimentally reproduce field seismic data with a great accuracy on small scale model. Figure 1 shows the bench and its components. MUSC system is composed of a honeycomb tab and two arms which control the source and the receiver position with a precision of $10\text{ }\mu\text{m}$.

The receiving system of MUSC system is a laser interferometer. The principle of this laser is based on a phase shift of the reflected laser signal due to the wave propagation in the material. A real-time calibration value enables a continuous conversion to a nanometric displacement. The focal diameter of the laser on the model surface is about several micrometers and allows a detection limit of 2.5 nm (few) in the frequency range from 30 kHz to 20 MHz .

The seismic source is simulated by a piezoelectric transducer relied to a launching and synchronization system. This system provides more energy than a laser impulse source (Bretaudeau, 2010; Bretaudeau et al., 2011) and allows to choose the source function, *i.e.*, Gauss source, Ricker source, central frequency f_0 and time delay t_0 . The source is generated by a waveform generator and is then amplified before transmitted to the small-scale-model.

In the framework of seismic physical modeling, the source must be as closed as possible to a normal point source. Thus, the piezoelectric source is coupled with an adapter in order to reproduce the spatial energy repartition (limiting directivity) and conserving the waveform
70 as shown in figure 3.

For the purpose of small scale modeling, the change of scale must keep the relationship between observables. For most of seismic imaging methods, the significant physical parameters are the compressional and shear waves velocities, V_P and V_S respectively, the density ρ and the quality factor Q . When scaling the model, many parameters can be modified:
75 the distances, the time scale, the amplitudes of the signals, the viscoelastic properties, etc. Hence, the predominant factor is the wavelength $\lambda = V/f$, where V is the wave velocity and f the frequency. Thus, physical and mechanical parameters are modified to preserve the ratio $\lambda_{real} = \xi \lambda_{scale}$ where ξ is the scale ratio. It is therefore necessary to act directly on the time-frequency scales. Assuming the materials used to build the small scale model have
80 the same mechanical properties (V_P , V_S , ρ) than the natural media, it is straightforward to obtain the scale ratios for parameters involved in seismic experiment.

For near surface experiments, the scale ratio ξ is about 1000 which means that the central frequency f_0 of the source is few kHz (generally 100 kHz but can be more or less), distances are in mm (acquisition length around 50 mm typically) and time unit is ms . (V_P , V_S etc...)
85 Small-scale models are generally made of metal, thermoplastic or melted epoxy resin-based materials (Bretaudeau et al., 2013, 2011, 2008). These materials allow to reproduce complex geometries and have a large panel of physical and mechanical properties. These materials have the advantages to have physical properties closed to natural soil materials after scaling. The models are generally over-sized to easily separate reflected waves on boundaries from

90 the rest of the signal.

Numerical modeling: Spectral Element Method

Various numerical methods exist to resolve the equation of motion in arbitrary elastic media. The most widely used is the Finite-Differences (FD) method (Virieux, 1986; Levander, 1988; Robertsson et al., 1994; Pratt, 1990; Stekl and Pratt, 1998; Saenger and Bohlen, 2004) which
95 estimates each derivative on a regular Cartesian grid using a Taylor development (Moczo et al., 2004) of order n . FD is simple to implement but quickly shows some limitations: the Cartesian grid is defined by the minimum propagated wavelength (λ_{min}) in the full media and is unable to reproduce properly complex topography and interfaces. Moreover, Saenger et al. (2000) show that 60 points by wavelength (λ) are needed to model propagation of
100 Rayleigh wave in order $n = 2$ where only 15 points by λ are required to model propagation of body waves which increases drastically the numerical cost in case of near-surface modeling experiment. The Finite-Elements Method (FEM) is another popular method used for wave propagation modeling (Lysmer and Drake, 1972; Seron et al., 1990; Hulbert and Hughes, 1990). FEM is based on a variational formulation of the equation of motion and gives a
105 continuous approximate solution in space using polynomial basis functions defined on each node of each cell of the mesh. The natural boundary conditions of FEM is the free surface and the triangular (in 2D) or tetraedric (in 3D) unstructured meshes are well adapted to complex media and topography. However, low polynomial basis are inadequate with fine spatial discretization and the required discretization to obtain precise and non-dispersive
110 solution is numerically costly.

Recently, the Spectral Element Method (SEM), widely used in fluid dynamics (Patera, 1984;

Korczak and Patera, 1986; Karniadakis, 1989), was adapted to seismic wave propagation (Komatitsch et al., 1998; Komatitsch and Tromp, 1999; Komatitsch et al., 2005; Festa and Vilotte, 2005).

115 The SEM is based upon a high-order piecewise polynomial approximation of the weak formulation of the wave equation. It combines the accuracy of the pseudo-spectral method with the flexibility of the finite-element method (Tromp et al., 2008).

In this method, the wave-field is represented in terms of high-degree Lagrange interpolants, and integrals are computed based upon Gauss-Lobatto-Legendre (gll) quadrature. This
120 combination leading to a perfectly diagonal mass matrix leads in turn to a fully explicit time scheme which leads itself very well to numerical simulations on parallel computers. It is particularly well suited to handling complex geometries and interface matching conditions (Cristini and Komatitsch, 2012).

As in FEM, all boundary of the domain are reflecting and the free surface is the natural
125 condition. In order to simulate infinite or semi-infinite domain, SEM can use Perfect Match Layers boundary conditions (Bérenger, 1994; Festa and Vilotte, 2005) but are not used here.

The typical element size that is required to generate an accurate mesh is of the order of λ , λ being the smallest wavelength of waves traveling in the model.

Models are meshed in 2D with quadrangles using the open-source software package GMSH
130 (Geuzaine and Remacle, 2009).

RESULTS

From point-source to line-source response

In the framework of wave propagation modeling and waveform inversion, most of available algorithms are limited to the two-dimensional approximation especially for computational cost causes. Thus, line-source seismograms are required as observed data to be compared
135 to synthetic seismograms or for inversion processes.

However, MUSC system is designed to produce three-dimensional experimental seismograms from a piezoelectric source selected to be as closed as possible to a point source. Generally, the correction of the geometrical spreading is done by convolving each trace by $\sqrt{t^{-1}}$, where t is the travel-time, with or without offset conditioning. The correct phase can then
140 be obtained using a source wavelet estimation method (Bretaudeau et al., 2011).

Recently, Forbriger et al. (2014) and Schafer et al. (2014) have developed, and successfully applied to synthetic seismograms, an hybrid method to convert the three-dimensional geometrical spreading in two-dimensional spreading using both convolution tapering and offset dependent scaling of the waveform. However, these pre-processing methods are not
145 perfect and can not be easily automated and the results are strongly conditioned by user's experience and attempts.

Here, we take advantage of the experimental framework to explore an alternative approach specific to MUSC system. Contrary to field experiments, it is possible to generate a pseudo-line-source finely sampled by multiple point-sources, perpendicular to the acquisition line.
150 Each point-source must be enough close to each other so the resulting source being a line-source in the sense of Huygens principle. To do that, we consider that the length of the

line must be equal, at least, $L \geq 4\lambda_{max}$ and the sampling interval $ds \leq 10/\lambda_{min}$. Given the material's properties, we choose $L = 240 \text{ mm}$ and $ds = 0.5 \text{ mm}$ which leads to 481 point-source locations. The line of point-source is located at ?? mm distance. Four receiver
155 positions have been selected: 45, 50, 55 and 60 mm offset perpendicular to the line-source. The source wavelet is a Ricker with a central frequency $f_0 = 100 \text{ kHz}$. Each receiver is perpendicular to and centered on the line-source. For each receiver position, the complete signal is stack along source position to obtain an equivalent two-dimensional line-source response.

160 To evaluate the efficiency of the method, experimental line-source responses will be compared to point-source and equivalent line-source responses using the cross-correlation coefficient (**cc**) and the root mean square (**rms**) ratio. These values are presented in table 2. **cc_{init}** and **rms_{init}** correspond to direct evaluation whereas **cc_{final}** corresponds to the best **cc** obtained and **rms_{final}** is the corresponding **rms**.

165 Figures 8(a) show the comparison between experimental traces obtained using a point-source and a line-source for source-receiver offsets 50, 55, 60 and 65 mm respectively. It is straightforward that these waveforms are not similar in terms of both phases (**cc**<0.75) and amplitude (**rms**>0.4). Even after amplitude fitting, point-source response to the line-response in term of phase (**cc**<0.8), amplitudes do not match (**rms**>0.4). These results
170 confirm that using raw point-source responses in a two-dimensional inversion process or imaging method can be critical in terms of convergence and validity of the results since these methods are built over phase and/or amplitude similarity.

Figures 8(b) show the comparison between experimental traces using a line-source and a point-source after geometrical spreading corrections (equivalent line-source response) for

175 the same previous source-receiver offsets. The cross-correlation coefficient **cc** for these waveforms are greater than 0.95 and $\text{rms} < 0.25$. These results denote that the experimental line-source response is correct in terms of phase compared to an equivalent line-source response. However, **rms** are quite great even if they are smaller than previously. This can be explained by small differences in terms of waveforms and phases which are critical in the
180 final **rms** results. Moreover, the *hybrid* method to obtain the equivalent line-source response from a point-source response needs accurate parametrization to obtain the best result which is not necessarily in a good agreement with the attempt true line-source response.

These results show that the line-source emulation on the MUSC system is efficient and can produce data suitable for imaging methods such as 2D FWI.

185 **Experimental source reproducibility**

To assess the ability of MUSC system to provide reproducible data, *i.e.* to evaluate the reproducibility of the source impact, several physical modeling were performed on a homogeneous epoxy-resin block for which the seismic waves velocities and the intrinsic attenuation are known : $V_P = 2300 \text{ m.s}^{-1}$, $V_S = 1030 \text{ m.s}^{-1}$, $\rho = 1300 \text{ kg.m}^{-3}$ and $Q = 30$.

190 Ten realizations have been acquired on this model with a similar geometry setup, *i.e.* 120 receivers positions with an increment equal to 1 mm and a minimum offset of 10 mm. The numerical wavelet sent to the piezoelectric transducer source is a Ricker signal with a central frequency of 100 kHz. However, the source waveform is modified by the physical coupling effect of the transducer.

195 First, a mean receiver-gather was calculated from the ten realizations and each trace of each realization was compared to equivalent one from mean receiver-gather. Figure 9 shows the

central traces of each realization and **cc** gives the correlation coefficient between each central trace with the central trace of the mean receiver-gather. The **cc** are always greater than 0.98 which demonstrate the high reproducibility of MUSC system experiments. However,
200 traces are not exactly the same which denotes a variability of the source from an experiment to another.

In a second step, a unique source wavelet is estimated using a linear source wavelet estimation method based on a stabilized deconvolution (Pratt, 1999). The source wavelet estimation takes into account the ten experiments together and allows to obtain a mean
205 effective source suitable for each experiment. The resulting source wavelet is applied to the synthetic signals (figure 10). The corrected seismograms are in good agreement with the experimental seismograms (correlation coefficients > 0.96) confirms the great efficiency of the wavelet source assessment process.

These last results, based on an average estimated source wavelet show that the effective
210 impulse source emitted by the transducer in the MUSC system measurement bench is stable enough to ensure a robust reproducibility of the source. Therefore, concerning the key issue of the source knowledge, experimental data acquired in the MUSC system can be efficiently processed by imaging methods like Full Waveform Inversion (FWI) with only one estimation step for all the multi-source and multi-receivers data.

215 To go further, we can imagine that the source correspond to the transducer-model coupling. So, an other model containing F50 pure epoxy-resin at the source position should have the same transmitted source wavelet....

Figure 11 shows the comparison between experiment data (black) and numerical data using the previously estimated source (red)...

CONCLUSIONS

220 These two studies allow to refine the capacity of the physical modeling designed for seismic
experiments simulation by 1) completing the validation of the measurement through com-
parison of numerical and experimental data generated by a realistic 2D source line and 2)
assessing the reproductivity of the effective source emitted in a model. These improvements
allow to provide and distribute experimental reduced scale data to the scientific community
225 as benchmark datasets.

PLOTS

Equations

Figures

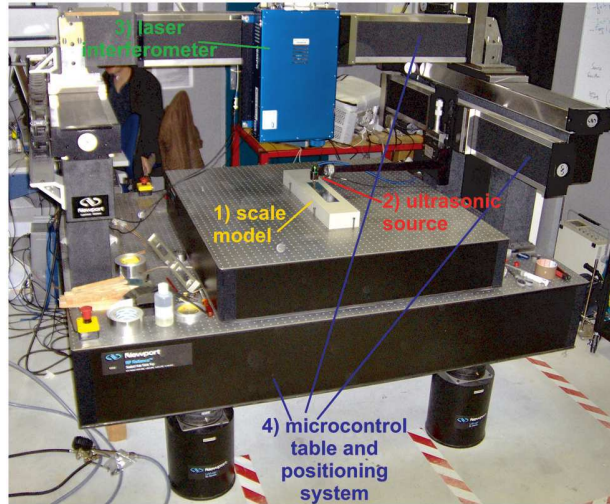


Figure 1: Photograph of the MUSC ultrasonic laboratory (from Bretaudeau et al. (2013)) with its four components: (1) a small-scale model of the underground, (2) an optical table with two automated arms moving above the model, (3) a laser interferometer recording ultrasonic wave propagation at the model surface, and (4) a piezoelectric ultrasonic source generating ultrasonic waves in the model.

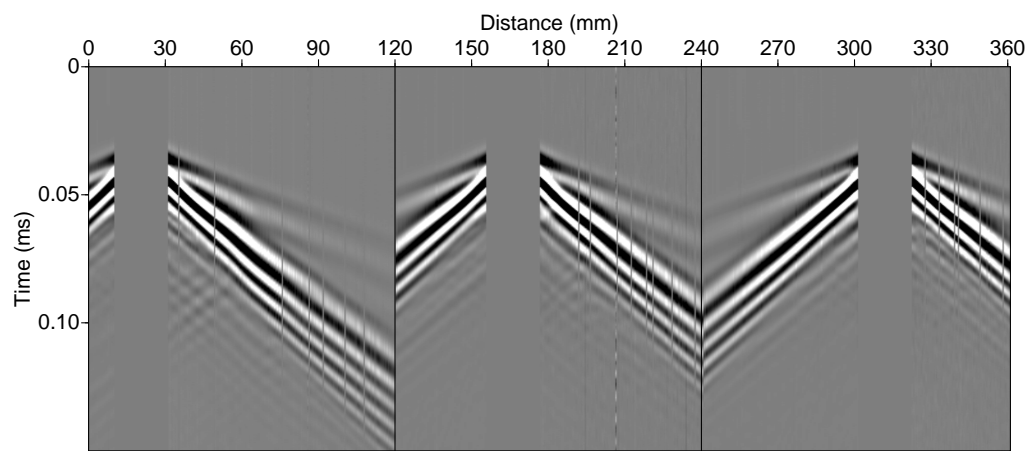


Figure 2: Example of multi-source multi-receiver record on the MUSC system for a two-layer model (balt).

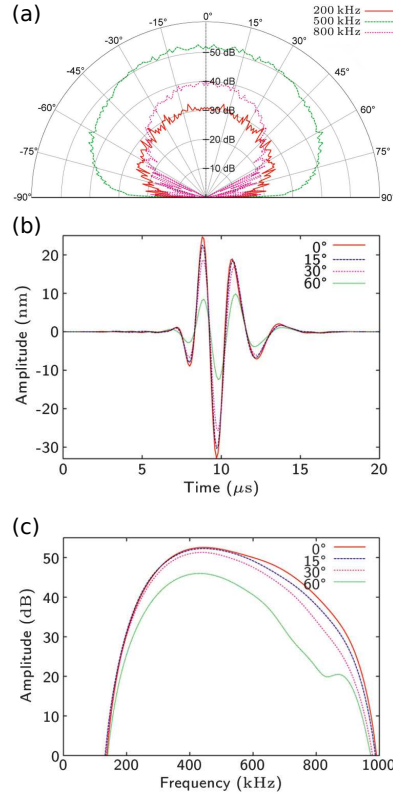
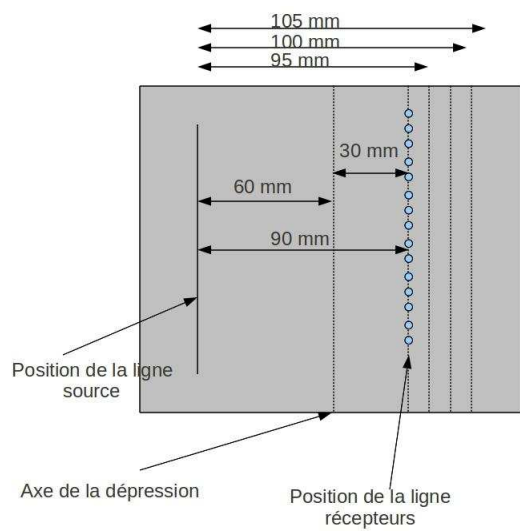
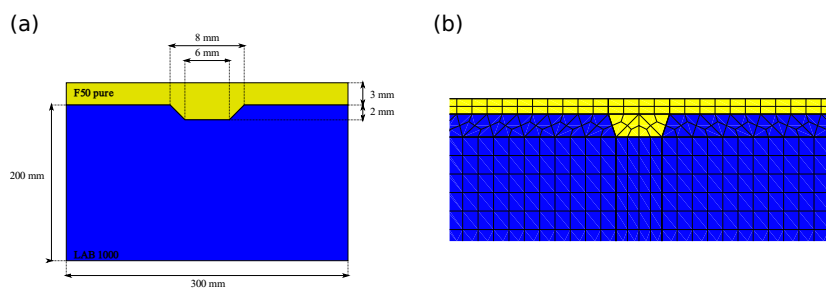


Figure 3: Validation of the piezoelectric source coupled with an adapter (Bretaudeau et al., 2011). (a) Directivity diagrams (dB) for the high-frequency source Panametrics® with conical polyurethane adapter: three frequencies normal particle displacement. (b) Temporal signals and (c) amplitude spectrums for the high-frequency source Panametrics® with a conical polyurethane adapter in transmission through a PVC cylinder for various angles of incidence: 0, 15, 30, and 60 degrees normal particle displacement.



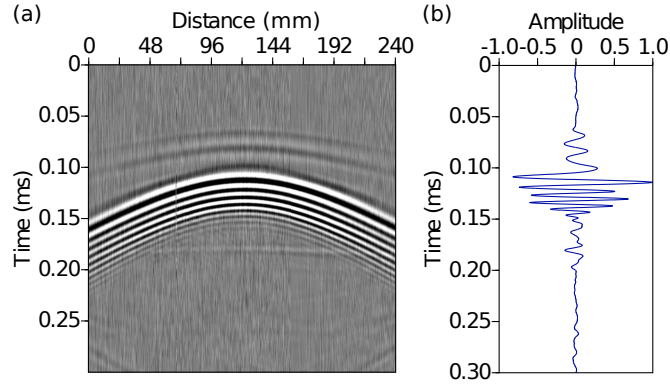


Figure 6: .

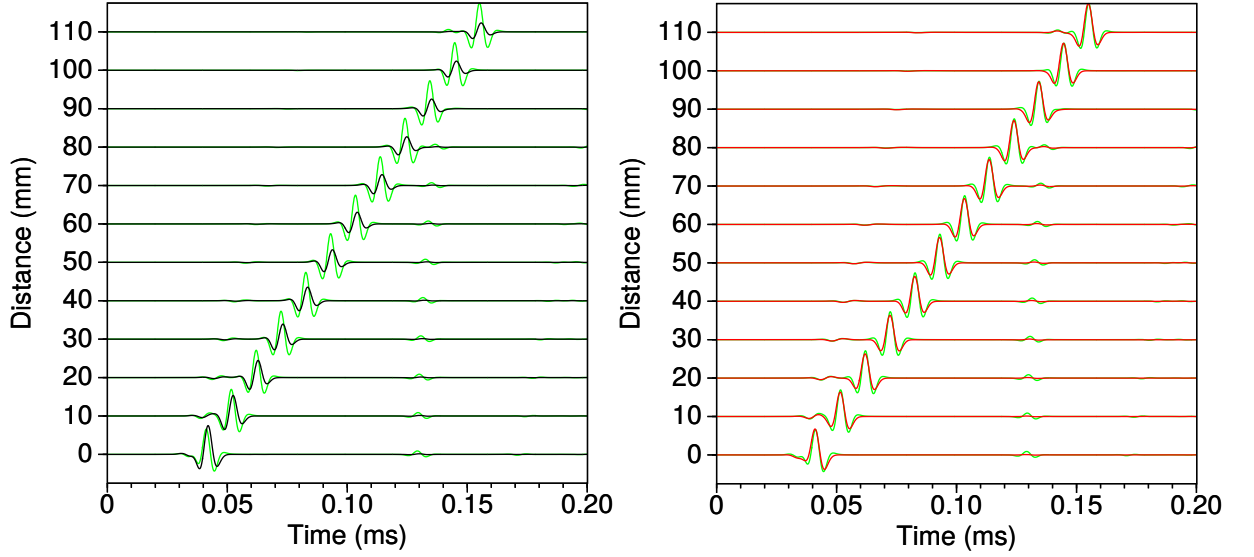


Figure 7: (a) Comparison between an experimental seismogram for a point-source (red) and for a line source (black), for 50, 55, 60 and 65 mm source-receiver offsets respectively. (b) Comparison between an experimental seismogram for a line-source (black), and a point-source response corrected from geometrical spreading (green) for same source-receiver offsets as (a). **cc** gives the correlation factor between line-source and point-source responses.

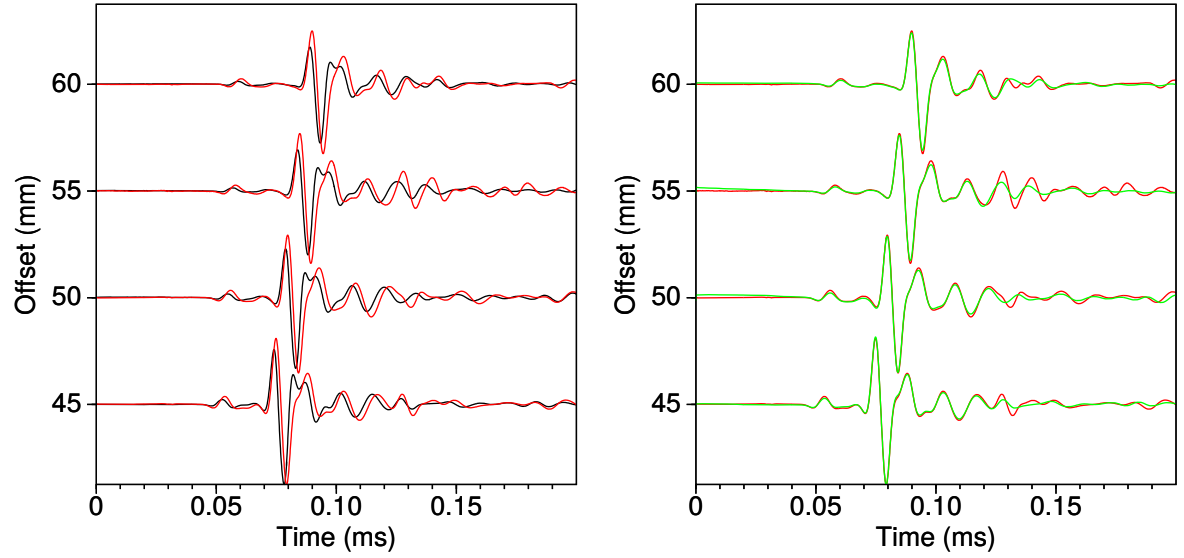


Figure 8: (a) Comparison between an experimental seismogram for a point-source (red) and for a line source (black), for 50, 55, 60 and 65 mm source-receiver offsets respectively. (b) Comparison between an experimental seismogram for a line-source (black), and a point-source response corrected from geometrical spreading (green) for same source-receiver offsets as (a). **cc** gives the correlation factor between line-source and point-source responses.

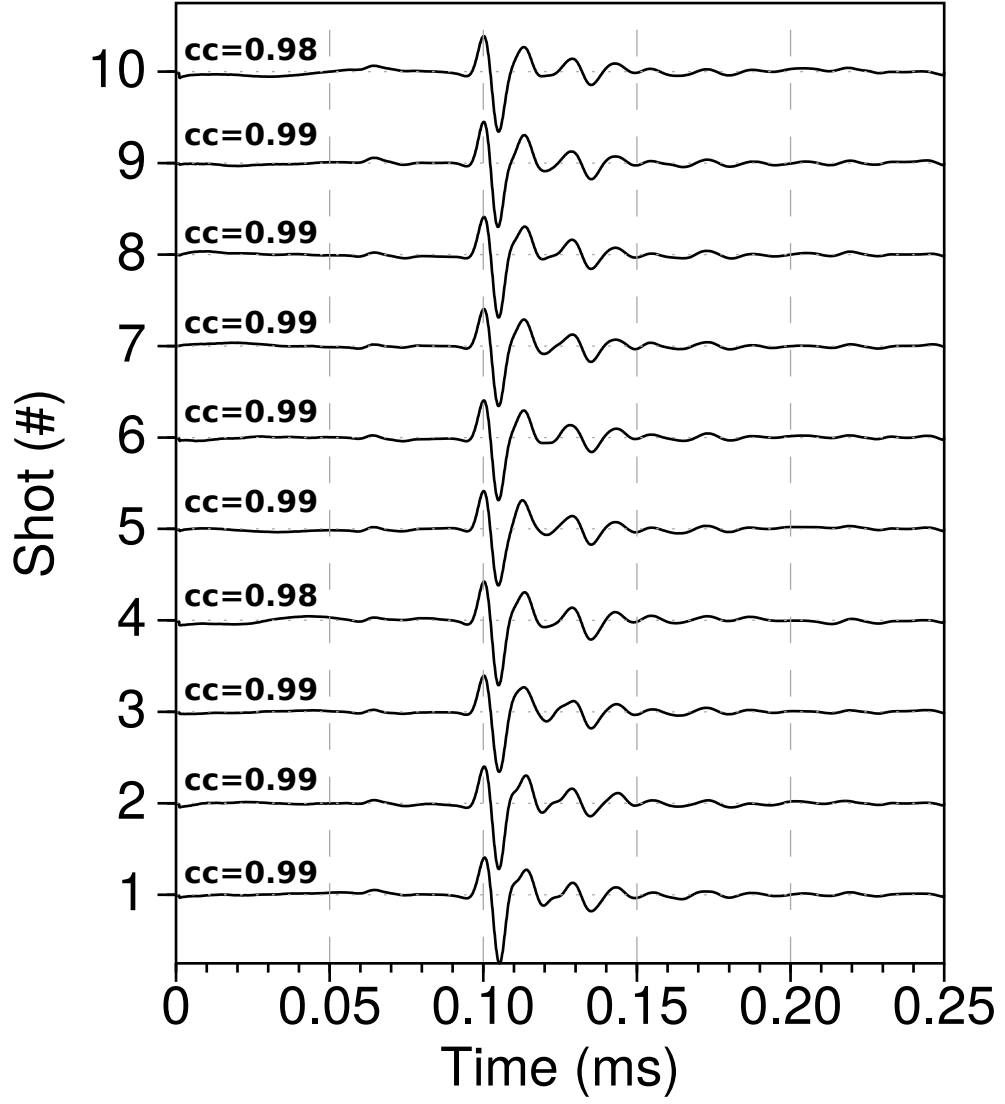


Figure 9: Central trace for each of the ten analogic experiment. `cc` gives the correlation factor of each central trace with respect to a mean trace.

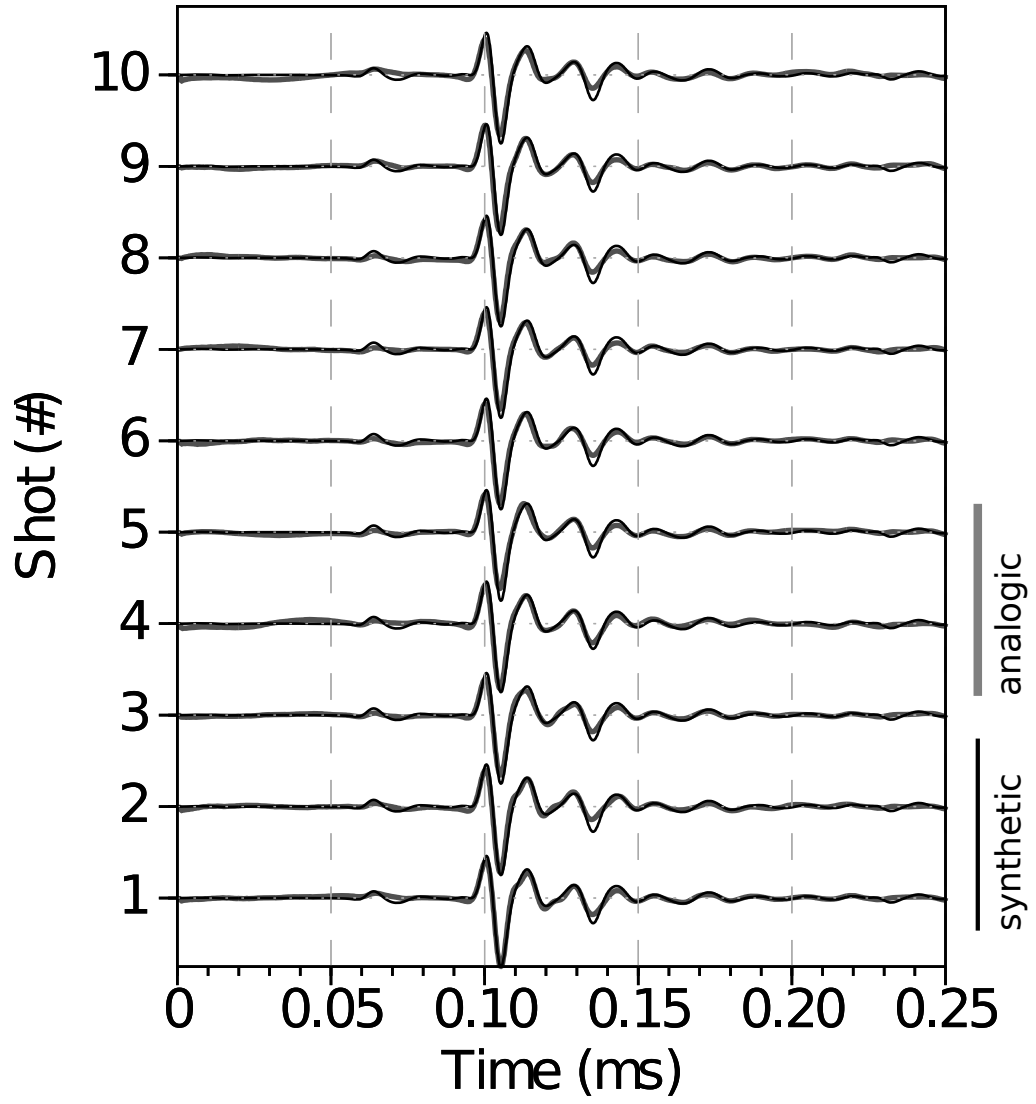


Figure 10: Comparison between analogic central traces (grey) and numerical traces corrected from the estimated effective source (black) for each experiment. **cc** gives the correlation coefficient.

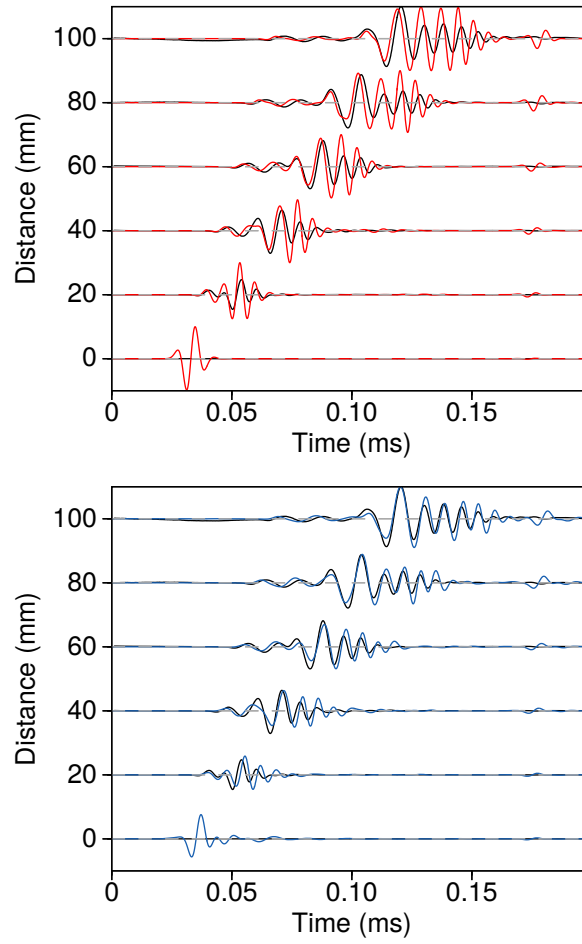


Figure 11: .

Tables

material	V_P (m/s)	V_S (m/s)	V_R (m/s)	ρ (kg/m ³)	Q
Aluminium	5630	3225	–	2700	–
F50 pure	2300	1030	965	1300	30
F50 200%	2820	1425	1328	1766	–
F50 240%	2968	1496	1388	1822	–
LAB1000	2850	1400	1310	1500	75

Table 1: Physical properties of some materials used to build small scale models. V_P , V_S and V_R are the P-wave velocity, S-wave and the Rayleigh wave velocity, respectively. ρ is the density and Q is the quality factor.

	90 mm	95 mm	100 mm	105 mm
$cc1_{init}$	0.702	0.725	0.728	0.728
$rms1_{init}$	0.794	0.760	0.762	0.774
$cc1_{final}$	0.940	0.953	0.951	0.949
$rms1_{final}$	0.358	0.317	0.325	0.343
$cc2_{init}$	0.954	0.987	0.988	0.988
$rms2_{init}$	0.304	0.162	0.155	0.154
$cc2_{final}$	—	—	—	—
$rms2_{final}$	—	—	—	—

Table 2: .

ACKNOWLEDGMENTS

REFERENCES

- Bérenger, J. P., 1994, A perfectly matched layer for the absorption of electromagnetic waves:
230 Journal of Computational Physics, **114**, 185–200.
- Berkhout, A., D. Verschuur, and G. Blacquiere, 2012, Illumination properties and imaging
promises of blended, multiple-scattering seismic data: a tutorial: Geophysical Prospecting,
60, 713–732.
- Bishop, T., K. Bube, R. Cutler, R. Langan, P. Love, J. Resnick, R. Shuey, and D. Spinder,
235 der, 1985, Tomographic determination of velocity and depth in laterally varying media:
Geophysics, **50**, 903–923.
- Bohm, G., J. M. Carcione, D. Gei, S. Picotti, and A. Michelini, 2015, Cross-well seismic
and electromagnetic tomography for CO₂ detection and monitoring in a saline aquifer:
Journal of Petroleum Science and Engineering, **133**, 245–257.
- 240 Bretaudeau, F., 2010, Modélisation physique à échelle réduite pour l’adaptation de
l’inversion des formes d’ondes sismiques au génie civil et à la subsurface: PhD thesis,
Université de Nantes.
- Bretaudeau, F., R. Brossier, D. Leparoux, O. Abraham, and J. Virieux, 2013, 2d elastic full-
waveform imaging of the near-surface: application to synthetic and physical modelling
245 data sets: Near Surface Geophysics.
- Bretaudeau, F., D. Leparoux, and O. Abraham, 2008, Small scale adaptation of the seismic
full waveform inversion method - application to civil engineering applications.: The
Journal of the Acoustical Society of America, **123**.
- Bretaudeau, F., D. Leparoux, O. Durand, and O. Abraham, 2011, Small-scale modeling of
250 onshore seismic experiment: A tool to validate numerical modeling and seismic imaging
methods: Geophysics, **76(5)**, T101–T112.

- Cristini, P., and D. Komatitsch, 2012, Some illustrative examples of the use of the spectral-element method in ocean acoustics.: *Journal of the Acoustical Society of America*.
- Favretto-Cristini, N., A. Tantsereva, P. Cristini, B. Ursin, D. Komatitsch, and A. Aizenberg, 2013, Numerical modeling of zero-offset laboratory data in a strong topographic environment: results for a spectral-element method and a discretized kirchhoff integral method: *Earthquake Science*.
- Festa, G., and J. Vilotte, 2005, The Newmark as velocity-stress time-staggering: an efficient PML implementation for spectral element ssimulation of elastodynamics: *Geophysical Journal International*, **161**, 798–812.
- Forbriger, T., L. Gross, and M. Schafer, 2014, Line-source simulation for shallow-seismic data. part 1: theoretical background: *Geophysical Journal International*, **198**, 1387–1404.
- French, W. S., 1974, Two-dimensional and three-dimensional migration of model-experiment reflection profiles: *Geophysics*, **39(3)**, 265–277.
- Geuzaine, C., and J. Remacle, 2009, Gmsh: a three-dimensional finite element mesh generator with built-in pre- and post-processing facilities.: *International Journal for Numerical Methods in Engineering*, **79**, 1309–1331.
- Guofeng, L., L. Yaning, R. Li, and M. Xiaohong, 2013, 3d seismic reverse time migration on gpgpu: *Computers & Geosciences*, **59**, 10–23.
- Hilterman, F., 1970, Three-dimensional seismic modeling: *Geophysics*, **35**, 1020–1037.
- Howes, E., L. Tejada-Flores, and L. Randolph, 1953, Seismic model study: *Journal of the Acoustical Society of America*, **25**, 915–921.
- Hulbert, G. M., and T. J. Hughes, 1990, Space-time finite element methods for second-order hyperbolic equations: *Computer Methods in Applied Mechanics and Engineering*, **84**, 327–348.

- Isaac, J. H., and D. C. Lawton, 1999, Image mispositioning due to dipping media: A physical seismic modeling study: *Geophysics*, **64**, 1230–1238.
- Karniadakis, G. E., 1989, Spectral element simulations of laminar and turbulent flows in complex geometries: *Applied Numerical Mathematics*, **6**, 85 – 105. (Special Issue on Spectral Multi-Domain Methods).
- Komatitsch, D., and J. Tromp, 1999, Introduction to the spectral-element method for three-dimensional seismic wave propagation: *Geophysical Journal International*, **139**, 806–822.
- Komatitsch, D., S. Tsuboi, and J. Tromp, 2005, The spectral-element method in seismology.
- Komatitsch, D., J. P. Vilotte, R. Vai, J. M. Castillo-Covarrubias, and F. J. Sánchez-Sesma, 1998, The Spectral Element Method for Elastic Wave Equation: Application to 2-D and 3-D Seismic Problems: *International Journal for Numerical Methods in Engineering*, **45**, 1139–1164.
- Korczak, K. Z., and A. T. Patera, 1986, An isoparametric spectral element method for solution of the navier-stokes equations in complex geometry: *Journal of Computational Physics*, **62**, 361 – 382.
- Levander, A., 1988, Fourth-order finite-difference p-sv seismograms: *Geophysics*, **53**, 1425–1436.
- Lysmer, J., and L. A. Drake, 1972, A finite element method for seismology: *Methods in computational physics*, **11**, 181–216.
- Moczo, P., J. Kristek, and L. Halada, 2004, The finite-differences method for seismologists: An introduction: Comenius University, Bratislava.
- Patera, A. T., 1984, A spectral element method for fluid dynamics: Laminar flow in a channel expansion: *Journal of Computational Physics*, **54**, 468–488.
- Perez Solano, C., D. Donno, and H. Chauris, 2014, Alternative waveform inversion for

- 300 surface wave analysis in 2-d media: *Geophysical Journal International*, **198**, 1359–1372.
- Pratt, R. G., 1990, Frequency domain elastic wave modeling by finite differences: A tool for cross-hole seismic imaging.: *Geophysics*, **55**, 626–632.
- , 1999, Seismic waveform inversion in the frequency domain, Part 1: Theory and verification in a physical scale model: *Geophysics*, **64**, 888–901.
- 305 Rieber, F., 1936, Visual presentation of elastic wave patterns under various structural conditions: *Geophysics*, **1**, 196–218.
- Robertsson, J., J. Blanch, and W. Symes, 1994, Viscoelastic finite-difference modeling.: *Geophysics*, **59**, 1444–1456.
- Saenger, E. H., and T. Bohlen, 2004, Finite-difference modeling of viscoelastic and anisotropic wave propagation using the rotated staggered grid: *Geophysics*, **69**, 583–591.
- 310 Saenger, E. H., N. Gold, and A. Shapiro, 2000, Modeling the propagation of elastic waves using a modified finite-difference grid: *Wave Motion*, **31**, 77–92.
- Sarkar, D., A. Bakulin, and R. L. Kranz, 2003, Anisotropic inversion of seismic data for stressed media: Theory and a physical modeling study on berea sandstone: *Geophysics*,
 315 **68**, 1–15.
- Schafer, M., L. Gross, T. Forbriger, and T. Bohlen, 2014, Line-source simulation for shallow-seismic data. part2: full-waveform inversion – a synthetic 2-d case study: *Geophysical Journal International*, **198**, 1405–1418.
- Seron, F. J., F. J. Sanz, M. Kindelan, and J. I. Badal, 1990, Finite-element method for elastic wave propagation: *Communications in applied numerical methods*, **6**, 359–368.
- 320 Stekl, I., and R. G. Pratt, 1998, Accurate visco-elastic modeling by frequency-domain finite differences, using rotated operators.: *Geophysics*, **63**, 1779–1794.
- Tromp, J., D. Komatitsch, and Q. Liu, 2008, Spectral-element and adjoint methods in

seismology.: Commun Comput Phys.

325 Virieux, J., 1986, P-sv wave propagation in heterogeneous media: velocity-stress finite-difference method: Geophysics, **51**, 889–901.

Virieux, J., and S. Operto, 2009, An overview of full-waveform inversion in exploration geophysics: Geophysics, **74**, WCC1WCC26.

Wong, J., K. W. Hall, E. V. Gallant, R. Maier, M. Bertram, and D. C. Lawton, 2009,
330 Seismic physical modeling at university of calgary: CSEG recorder, **34**.